


Coexistence of Terrestrial and Satellite Networks in the 28-GHz Band

ANIQ UR RAHMAN 
University of Oxford, Oxford, U.K.

MUSTAFA A. KISHK , Member, IEEE
National University of Ireland, Maynooth, Ireland

MOHAMED-SLIM ALOUINI , Fellow, IEEE
King Abdullah University of Science and Technology, Thuwal, Saudi Arabia

We present a practical framework for maximizing the average data rates of terrestrial networks operating in the 28-GHz band while considering their coexistence with satellite networks. The 28-GHz mmWave band is licensed to fixed satellite services for Earth-to-space uplink transmissions, which are also used by the terrestrial cellular and backhaul networks for downlink operation. Our approach focuses on finding the optimal radii for exclusion zones, which are the areas where certain network elements are restricted from operating in the 28-GHz band. Through stochastic geometry, we derive the average data rate expressions for the terrestrial networks as functions of the exclusion zone radii of the Earth stations and the backhaul points. We then convert the discrete problem of frequency allocation into a continuous problem through Poisson point process approximation of the transmitters' locations. We perform logistic regression on the integral-form coverage probability expression to obtain closed-form approximation of the data rate expressions. This facilitates faster optimization, making our framework viable for deployment in frequency allocation systems, offering near-optimal results with lower complexity compared with combinatorial techniques. We improve the

Manuscript received 3 March 2023; revised 13 June 2023; accepted 1 August 2023. Date of publication 16 August 2023; date of current version 8 December 2023.

DOI. No. 10.1109/TAES.2023.3302819

Refereeing of this contribution was handled by A. Knopp.

The work was supported by the KAUST office of sponsored research.

Authors' addresses: Aniq Ur Rahman is with the Department of Engineering Science, University of Oxford, OX1 3PJ Oxford, U.K., E-mail: (aniq.rahman@eng.ox.ac.uk); Mustafa Kishk is with the Department of Electronic Engineering, National University of Ireland, W23 F2H6 Maynooth, Ireland, E-mail: (mustafa.kishk@mu.ie); Mohamed-Slim Alouini is with Computer, Electrical and Mathematical Sciences and Engineering Division, King Abdullah University of Science and Technology, Thuwal 23955-6900, Saudi Arabia, E-mail: (slim.alouini@kaust.edu.sa). (Corresponding author: Aniq Ur Rahman.)

0018-9251 © 2023 IEEE

data rate of cellular users by up to ~30% at the expense of the data rate of the backhaul points degrading by ~2%.

I. INTRODUCTION

As we move toward the 6G of connectivity, satellites have been identified as an indispensable solution to bridge the digital divide [1], [2]. The satellites offer a large coverage footprint [3] and can reach the most remote regions [4] with high throughput, fueled by the large bandwidth available in higher frequency bands.

Among the satellites, the geostationary satellites have the largest footprint; however, since they are furthest from the Earth, they have long delays [3], making them unsuitable for low-latency applications of 5G and beyond networks. To circumvent this problem, we could make use of a megaconstellation of low Earth orbit (LEO) satellites [5], [6], which have recently gained traction, as evident from the projects by Starlink, OneWeb, and Kepler, to name a few [7].

The push for integrating satellites into the future network architecture to complement the terrestrial networks is reasonable [7], given that connecting the global population through terrestrial networks alone is cost-prohibitive. However, there may be cases where the satellite and terrestrial networks compete for the same spectrum band, thereby being a source of interference for each other. This is an exciting problem, referred to as spectrum coexistence in the literature.

The mmWave bands have attracted the attention of LEO satellite networks and terrestrial mobile operators alike. Specifically, the 28-GHz mmWave band is licensed to fixed satellite services (FSSs) for Earth-to-satellite uplink transmissions [8], while the terrestrial networks will use it for downlink operation [9], [10]. The satellite networks are the primary users of the 28-GHz band (27.5–29.5-GHz). This band is vital for commercial satellite connectivity solutions and 5G nonterrestrial networks [11]. The 28-GHz band is also available for licensing to International Mobile Telecommunication (IMT) networks in countries, such as U.S., Canada, Norway, Australia, Japan, and Singapore [9]. In Latin America, Africa, and some countries in the Middle East, the 28-GHz band is used for point-to-multipoint wireless backhaul links [12].

In Fig. 1, we depict the signal and interference among the different networks' elements involved in our coexistence study.

We assume that the Earth stations (ESs) coordinate their transmissions so as not to cause strong interference to the LEO satellites. In our study, the focus is primarily on the terrestrial networks operating in the 28-GHz band. Therefore, to jointly maximize the data rates of the cellular and backhaul users, we determine the radii of the exclusion zones dictated by the ESs and backhaul points (BPs) to keep the terrestrial users out of high interference zones.

The rationale of our study is outlined in Fig. 2, where we assume that the location database of ESs, cellular base stations (BSs), and BPs is available to us. With the help of these databases, we approximate the transmitters' spatial distribution as independent Poisson point processes

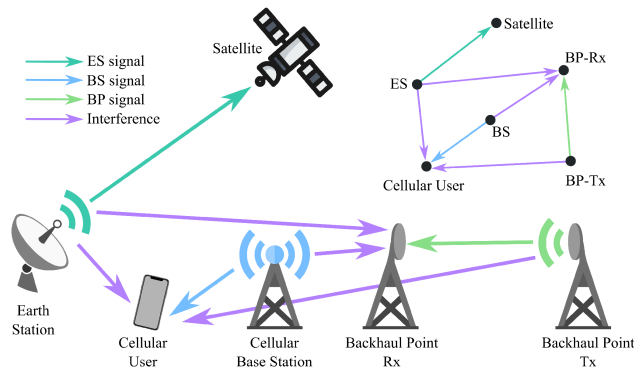


Fig. 1. Coexistence scenario of interest.

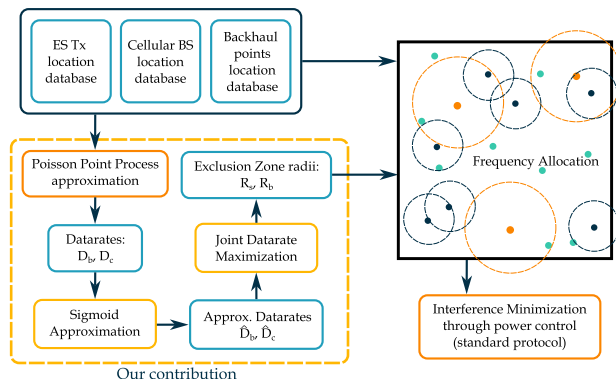


Fig. 2. Functional view of the coexistence system.

(PPPs) and derive the data rate expressions $\{D_c, D_b\}$ of the terrestrial networks using stochastic geometry that can be numerically evaluated but, unfortunately, are not closed form. Therefore, we first approximate the coverage probability expressions as sigmoid curves and obtain a closed-form expression for the data rates $\{\hat{D}_c, \hat{D}_b\}$, facilitating quicker analysis. Finally, we maximize the data rate expressions of the terrestrial networks jointly and obtain the optimum values of the exclusion zone radii $\{R_s, R_b\}$.

The main contributions of our work are given as follows.

- 1) We present a practical framework for maximizing the average data rates of the terrestrial networks operating in the 28-GHz band by finding the optimum radii of the exclusion zones.
- 2) Using stochastic geometry,¹ we derive the average data rate expressions of the terrestrial networks as a function of the exclusion zone radii of the ESs and BPs.
- 3) Allocating frequency² to different network elements is a discrete problem having exponential complexity; however, we convert it to a continuous problem through PPP approximation. Once the optimum values of the radii are determined, frequency allocation

¹Given the location database of different networks, we can approximate their positions as independent PPPs.

²Here, by frequency allocation, we mean that the transmitter operates in either 28 or 6 GHz/sub-6 GHz.

for a transmitter at any given location is a straightforward task.

- 4) To facilitate faster optimization, we approximate the data rate expressions in integral form as closed-form expressions by performing logistic regression on the coverage probability expressions.
- 5) The framework presented in this work has the potential to be used in practical frequency allocation systems as it performs near-optimal data rate maximization with lower complexity compared with combinatorial techniques.

II. RELATED WORKS

The coexistence of different technologies utilizing the same frequency band has always been a subject of interest for wireless researchers due to the ever increasing demand for spectrum resources.

A. Cognitive Radio (CR) for Coexistence

In CR [13] research, the focus is on managing the spectrum among various users that have different access rights to a given frequency band. CR networks rely heavily on spectrum sensing techniques [14] to assess the level of spectrum usage by primary users, which then allows to dynamically allocate [15] the available spectrum among the secondary users, while ensuring that the collective interference from the secondary users does not exceed a certain threshold [16]. In the recent literature on CR, the spectrum sensing and dynamic spectrum allocation tasks are being solved through machine learning [17] tools, such as deep learning [18], [19], [20] and reinforcement learning [21], [22], [23]. An alternative approach to model the interaction of different networks in a CR setup is through game theory [24], [25], [26].

B. Stochastic Geometry for Coexistence

Stochastic geometry is a valuable mathematical tool for analyzing wireless networks and deriving valuable performance insights [27]. It can capture the randomness in the network in terms of the spatial distribution of network elements as well as communication parameters, such as path loss, fading, and power control [28], [29]. Pinto et al. [30] use stochastic geometry to facilitate the coexistence of narrow-band and ultrawideband wireless networks. Mbengue and Chang [31] study the coexistence of license-assisted access of cellular networks and WiFi networks over unlicensed spectrum. The coverage probability of the two networks was derived using stochastic geometry. Similarly, Bhorakar et al. [32] use stochastic geometry to assess the performance of cellular and WiFi networks when they coexist in the 5-GHz unlicensed bands. Ur Rahman et al. [24] use stochastic geometry for quantifying the data rate of the cellular and WiFi networks using unlicensed 6-GHz band. The networks then play a noncooperative game to maximize their data rates, thereby achieving coexistence.

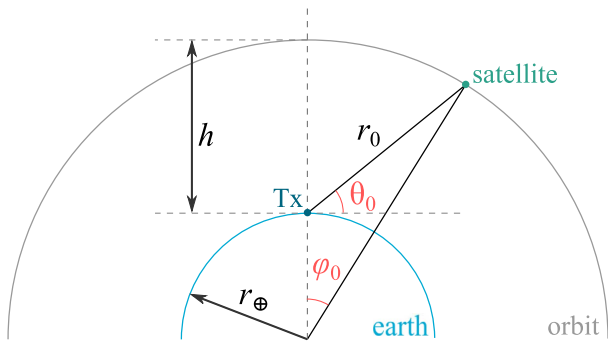


Fig. 3. Illustration of the geometric model.

C. Coexistence Through Exclusion Zones

Coexistence can be achieved either by temporal bandwidth slicing or by spatial segregation. In spatial coexistence [33], the goal is to maximize the separation between the users that use the same frequency bands. One way of achieving spatial coexistence is through exclusion zones [24]; the interference sources can be viewed as having a circular exclusion zone around them, the radius of which is referred to as the protection distance. The secondary users within the exclusion zones should not use the common spectrum, as the interference is high and will deteriorate performance. Kishk and Dhillon [34] use guard zones to improve the secrecy of the primary networks.

D. Coexistence of Satellite and Terrestrial Networks

Sharma et al. [35] use transmit beamforming for spectral coexistence of satellite and terrestrial networks. Here, the satellite links are in downlink toward the ground stations. In a similar setup, the work in [36] investigates the coexistence of 5G cellular BSs and FSSs in the C-band. Cho et al. [37] study the coexistence of 5G services with FSS in the mmWave bands of IMT-2020. Hassan et al. [38] assess the feasibility of coexistence between 5G and incumbent services in the IMT-2020 bands in Malaysia. The IMT-2020 bands primarily consist of mmWave bands, where one of the incumbents is FSSs. Cho et al. [39] investigate the spectral coexistence of IMT-2020 with FSS in the 28-GHz band. They calculate the minimum separation distances between the elements of the two coexisting networks; ESs and cellular BSs, to ensure good performance. Kime et al. [40] study the coexistence of 5G network with the incumbents in the 28-GHz and 70-GHz bands. They characterize the minimum separation between the ESs and cellular users in the order of a few kilometres in order to protect the cellular users from the ES interference. Zafar et al. [41] find the minimum protection distance between the terrestrial user and ES by varying the elevation angle of the FSS. They report that, for elevation angle below 37° , minimum protection distance greater than 100 m, while for elevation angle above 37° , protection distance lower than 100 m are sufficient to maintain a minimum signal-to-interference-plus-noise ratio (SINR) of

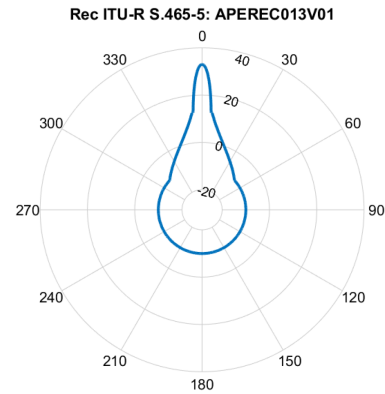


Fig. 4. Antenna pattern for ES transmitter operating in the 28-GHz band.

-8.8 dB. However both these works rely on deterministic setups, not taking into account the spatial randomness of network elements. Lin et al. [42] jointly maximize the secrecy and energy efficiency through beamforming, where satellite downlink and cellular downlink communication interfere with each other. A similar setup is investigated in [43], where Yan et al. maximize the outage-constrained achievable sum rate of all ESs under multicast downlink. In this work, we focus on frequency allocation, after which communication performance can definitely be enhanced through beamforming techniques, which is beyond our scope.

E. Stochastic Geometry for LEO Satellite Networks

The authors in [44] and [45] use stochastic geometry for downlink analysis of LEO satellite communication systems. Khan and Afshang [46] use stochastic geometry to characterize the Doppler shift in LEO satellite network. The work in [47] evaluates the accuracy of stochastic geometric models for LEO satellite networks, concluding that homogeneous binomial point process is a good approximation for orbit model point process, thereby mimicking the LEO constellations fairly well.

III. SYSTEM MODEL

In this section, we describe the satellite and terrestrial networks in detail, highlighting the design parameters which are used in the numerical derivations for performance analysis in Section IV.

A. Satellite Network

There are N satellites in the constellation, at an orbit height of h above the Earth's surface. The distance of the nearest satellite from the ES transmitter is r_0 . The elevation angle θ_0 is the angle between the tangent passing through the surface of the Earth at the ES transmitter and the direction of the nearest satellite (see Fig. 3).

The antenna pattern of 28-GHz transmitters [48], as seen in Fig. 4, is directional, and the angle that the boresight of the ES antenna makes with the terrestrial users while tracking

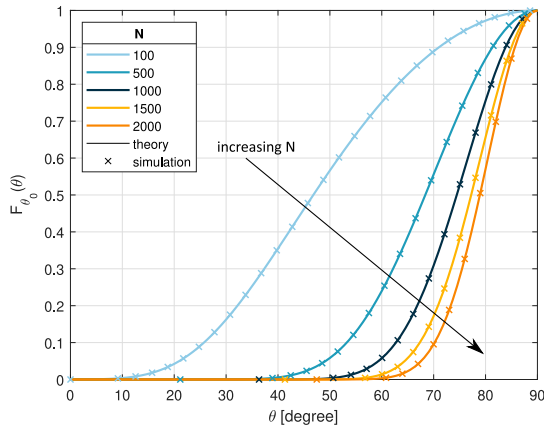


Fig. 5. Distribution of the elevation angle θ_0 , $h = 1000$ km.

the satellite changes with time. Therefore, we obtain the distribution of this interference angle, which helps us in capturing the interference from the sidelobes of the ESs accurately.

We know from [49, eq. (13)] that the contact angle φ_0 measured from the center of the Earth follows the distribution:

$$f_{\varphi_0}(\varphi) = \frac{N}{2} \sin \varphi \exp\left(-\frac{N}{2}(1 - \cos \varphi)\right). \quad (1)$$

Moreover, we can express the elevation angle θ_0 as a function of the contact angle φ_0 as follows:

$$\theta_0 = g(\varphi_0) = \tan^{-1}(\cot \varphi_0 - \gamma_1 \csc \varphi_0), \quad \gamma_1 = \frac{r_{\oplus}}{r_{\oplus} + h} \quad (2)$$

where r_{\oplus} denotes the radius of the Earth.

Conversely, we can express the contact angle φ_0 in terms of the elevation angle θ_0 as follows:

$$\varphi_0 = g^{-1}(\theta_0) = \cot^{-1}\left(\frac{\gamma_1^2 \tan \theta_0 + \sqrt{\gamma_1^2 \sec^2 \theta_0 - 1}}{\gamma_1^2 - 1}\right). \quad (3)$$

Therefore, the distribution of the elevation angle can be evaluated through transformation of random variable $\varphi_0 \rightarrow \theta_0$

$$f_{\theta_0}(\theta) = f_{\varphi_0}(g^{-1}(\theta)) \left| \frac{dg^{-1}(\theta)}{d\theta} \right|. \quad (4)$$

We verify the analytical result with Monte-Carlo simulations in Fig. 5 establishing that they are in agreement. As visible from the plot, the probability of having an elevation angle below 10° is almost negligible, and as the constellation gets denser, we see the probability dropping to zero even for the elevation angles of 40° – 55° . Therefore, our model adheres to the limits of the minimum elevation angle imposed by different operators [50], [51].

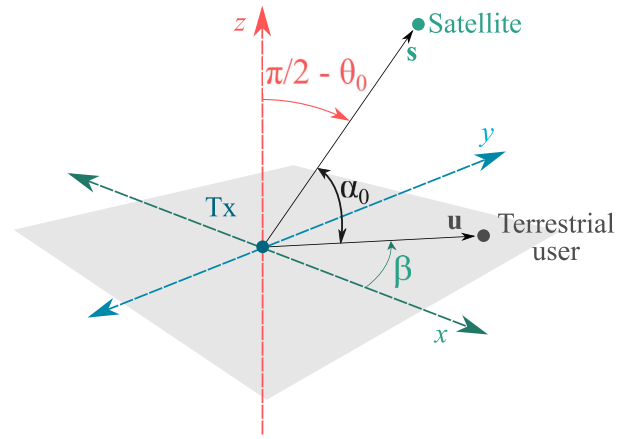


Fig. 6. Illustration of interference angle α_0 .

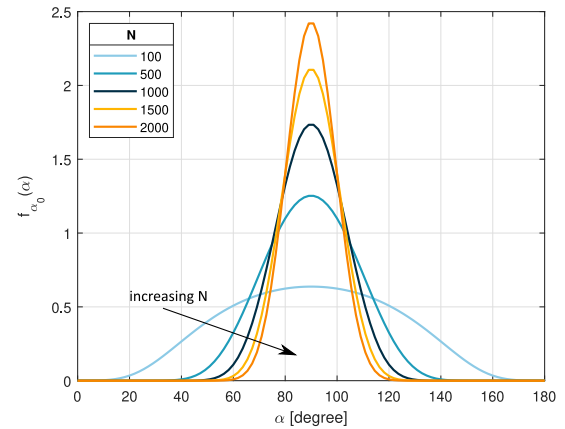


Fig. 7. Interference angle α_0 distribution, $h = 1000$ km.

To characterize the interference that the ES transmitters cause the terrestrial users, we need to find the distribution of interference angle α_0 (see Fig. 6).

DEFINITION 1 The angle that the terrestrial user \mathbf{u} makes with the boresight of the ES transmitter \mathbf{s} is defined as the interference angle α_0 .

$$\alpha_0 \triangleq \cos^{-1}(\cos \beta \cos \theta_0) \quad (5)$$

where $\beta \sim \mathcal{U}(0, 2\pi)$, and θ_0 is the elevation angle of the satellite with respect to the ES transmitter.

LEMMA 1 The distribution of the interference angle is

$$f_{\alpha_0}(\alpha) = |\sin \alpha| \int_{|\cos \alpha|}^1 \frac{f_{\theta_0}(\cos^{-1}(v))}{\pi \sqrt{(1-v^2)(v^2 - \cos^2 \alpha)}} dv. \quad (6)$$

The interference angle distribution is shown in Fig. 7. As the satellite density in the orbit increases, the boresight of the ES transmitter is pointed upward toward the sky, i.e., α_0 is close to $\pi/2$, which means that the terrestrial user (TUs) are affected primarily by the sidelobes of the ES transmitter.

B. Terrestrial Network

The space in \mathbb{R}^2 is populated by cofrequent ESs as a PPP with density λ_s , and each ES transmits at a power p_s .

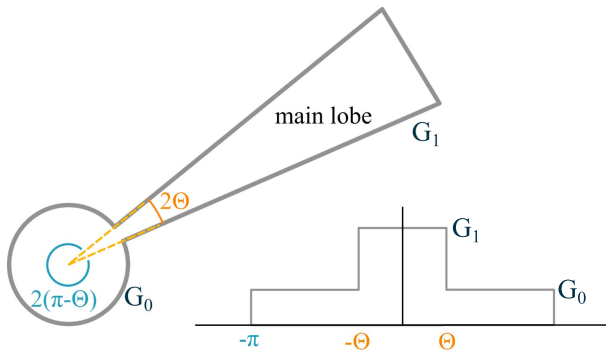


Fig. 8. Simplified antenna pattern for BP transmitters.

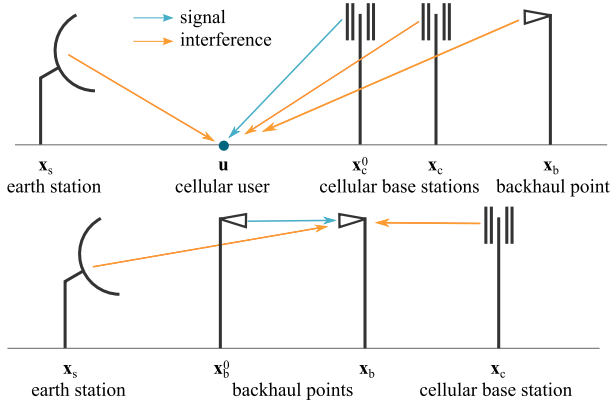


Fig. 9. Signal and interference for TUs.

Similarly, the BSs and BPs are distributed as two independent PPPs with densities λ_c and λ_b , respectively. We denote the PPPs describing the ESs, cellular BSs, and BPs with Φ_s , Φ_c , and Φ_b , respectively. Moreover, the BSs and BPs have transmit powers p_c and p_b , respectively. For wireless propagation of signal, we use Nakagami- m fading model, where m is the shape factor. We also assume free space path loss with $\zeta > 2$ as the path loss exponent. Since the ES transmitter antenna pattern is directional [48], the gain at an angle α measured from the main lobe is $G(\alpha)$ (see Fig. 4). Similarly, for the BP antenna, we consider a simplified two-lobe model, the main lobe has a beam width of 2Θ and gain G_1 , while the sidelobe has gain G_0 (see Fig. 8).

In Fig. 9, we depict the different sources of interference for each terrestrial user and formalize the same in the definitions that follow.

The power received by a cellular user at origin from a cellular BS at \mathbf{x} is $p_c H_{\mathbf{x}} \|\mathbf{x}\|^{-\zeta}$ and the power received by a BP from a backhaul transmitter at \mathbf{x} is $p_b G_1 H_{\mathbf{x}} \|\mathbf{x}\|^{-\zeta}$, where $H_{\mathbf{x}} \sim \Gamma(m, \frac{1}{m})$ is for Nakagami- m fading, and ζ is the path loss exponent. The interference from ESs is $I_s \triangleq \sum_{\mathbf{x} \in \Phi_s} H_{\mathbf{x}} G(\alpha) p_s \|\mathbf{x}\|^{-\zeta}$, and the interference from BPs is $I_b \triangleq \sum_{\mathbf{x} \in \Phi_b} H_{\mathbf{x}} G_{\mathbf{x}} p_b \|\mathbf{x}\|^{-\zeta}$. Moreover, the interference from the cellular BSs is $I_c \triangleq \sum_{\mathbf{x} \in \Phi_c} H_{\mathbf{x}} p_c \|\mathbf{x}\|^{-\zeta}$.

DEFINITION 2 The signal-to-interference ratio (SIR) experienced by a typical cellular user at the origin connected to

the nearest cellular BS at $\mathbf{x}_c^0 \in \Phi_c$ is

$$\text{SIR}_c \triangleq \frac{p_c H_{\mathbf{x}_c^0} \|\mathbf{x}_c^0\|^{-\zeta}}{I_c + I_s + I_b} \quad (7)$$

where I_c , I_s , and I_b denote the interference from the cellular BSs, ESs, and BPs, respectively.

DEFINITION 3 The SIR experienced by a typical BP at the origin connected to the nearest BP at $\mathbf{x}_b^0 \in \Phi_b$ is

$$\text{SIR}_b \triangleq \frac{p_b G_1 H_{\mathbf{x}_b^0} \|\mathbf{x}_b^0\|^{-\zeta}}{I_c + I_s + I_b^0} \quad (8)$$

where I_c , I_s , and I_b^0 denote the interference from the cellular BSs, ESs, and BPs, respectively.

IV. COVERAGE ANALYSIS

In order to determine coverage probability, we first need to characterize the interference from various sources, described by a random point process Φ . One way to do this is through Laplace transform of the interference I , defined as follows:

$$\mathcal{L}_I(s) \triangleq \mathbb{E}_{\Phi} [e^{-sI}] \quad (9)$$

which proves to be a useful tool in the mathematical analysis of networks. For example, to find the expectation of the interference $\mathbb{E}[I]$, we can write

$$\mathbb{E}_{\Phi}[I] = -\frac{\partial}{\partial s} \mathcal{L}_I(s) \Big|_{s=0}. \quad (10)$$

A. Laplace Transform of the Interference

The Laplace transform of the interference from various sources is presented in the Lemmas that follow, with the proofs deferred to Appendix A.

LEMMA 2 The Laplace transform of the interference from the ES transmitters described by a PPP of density λ_s is expressed as follows:

$$\mathcal{L}_{I_s}(s, v, \lambda_s) = \int_0^{\pi} \exp\left(-2\pi\lambda_s \int_v^{\infty} \left\{ 1 - \left(1 + \frac{G(\alpha)p_s x^{-\zeta}}{m} s\right)^{-m} \right\} x dx\right) f_{\alpha_0}(\alpha) d\alpha. \quad (11)$$

LEMMA 3 The Laplace transform of the interference from the BPs described by a PPP of density λ_b is expressed as follows:

$$\mathcal{L}_{I_b}(s, v, \lambda_b) = \exp\left(\mathbb{E}_G \left[-2\pi\lambda_b \int_v^{\infty} \left\{ 1 - \left(1 + \frac{G p_b x^{-\zeta}}{m} s\right)^{-m} \right\} x dx \right]\right) \quad (12)$$

where $f_G(G_1) = \frac{\Theta}{\pi}$ and $f_G(G_0) = 1 - \frac{\Theta}{\pi}$.

LEMMA 4 The Laplace transform of the interference from the cellular BSs described by a PPP of density λ_c is expressed as follows:

$$\mathcal{L}_{I_c}(s, v, \lambda_c) = \exp\left(-2\pi\lambda_c \times \int_v^\infty \left\{1 - \left(1 + \frac{p_c x^{-\zeta}}{m} s\right)^{-m}\right\} x dx\right). \quad (13)$$

B. Coverage Probability

Consequently, the coverage probability of the cellular users and BPs is expressed in Theorems 1 and 2, respectively. The proof is sketched on the same lines as [52, Appendix F], and is, therefore, skipped.

THEOREM 1 The coverage probability of the cellular users $\mathbb{P}(\text{SIR}_c > \tau)$ is

$$P_c(\tau) = 2\pi\lambda_c \sum_{k=1}^m \binom{m}{k} (-1)^{k+1} \int_0^\infty \exp(-\pi\lambda_c v^2) \times \mathcal{L}_{I_s}(\Omega_c, 0, \lambda_s) \mathcal{L}_{I_c}(\Omega_c, v, \lambda_c) \mathcal{L}_{I_b}(\Omega_c, 0, \lambda_b) v dv \quad (14)$$

where $\beta \triangleq (m!)^{-\frac{1}{m}}$ and $\Omega_c \triangleq \frac{k\beta m \tau v^\zeta}{\mu p_c}$.

THEOREM 2 The coverage probability of the BPs $\mathbb{P}(\text{SIR}_b > \tau)$ is

$$P_b(\tau) = 2\pi\lambda_b \sum_{k=1}^m \binom{m}{k} (-1)^{k+1} \int_0^\infty \exp(-\pi\lambda_b v^2) \times \mathcal{L}_{I_s}(\Omega_b, 0, \lambda_s) \mathcal{L}_{I_c}(\Omega_b, 0, \lambda_c) \mathcal{L}_{I_b}(\Omega_b, v, \lambda_b) v dv \quad (15)$$

where $\beta \triangleq (m!)^{-\frac{1}{m}}$ and $\Omega_b \triangleq \frac{k\beta m \tau v^\zeta}{\mu p_b G_1}$.

It can be seen from (14) and (15) that the performance of the terrestrial networks is interdependent on the transmission parameters and deployment density of the terrestrial as well as satellite uplink network. In Section V, we introduce the concept of exclusion zones and restate the coverage probabilities as a result of the introduction of such zones, and see how controlling the radius of these exclusion zones can result in performance gains for each terrestrial network involved.

V. EXCLUSION ZONE

To protect the TUs from ES transmissions, we create an exclusion zone of radius R_s around ESs within which the TUs do not operate in 28 GHz. Moreover, we encircle the BPs with an exclusion zone of their own of radius R_b within which the cellular users are not allowed to operate in the 28-GHz band. This is graphically depicted in Fig. 10, where the exclusion zones divide the space in \mathbb{R}^2 into four regions denoted by Roman numerals I–IV. The frequency usage by the TUs in these regions is tabulated in Table I.

Based on the new frequency usage rules presented in Table I, the density of the PPP describing the cellular BSs

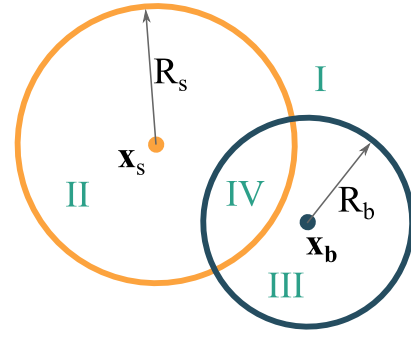


Fig. 10. Different regions created as a result of ESs and BPs having exclusion zones.

TABLE I
Frequency Usage by the TUs Based on the Region

Region	Cellular users	Backhaul points
I	28 GHz + sub-6 GHz	28 GHz + 6 GHz
II	sub-6 GHz	6 GHz
III	sub-6 GHz	28 GHz + 6 GHz
IV	sub-6 GHz	6 GHz

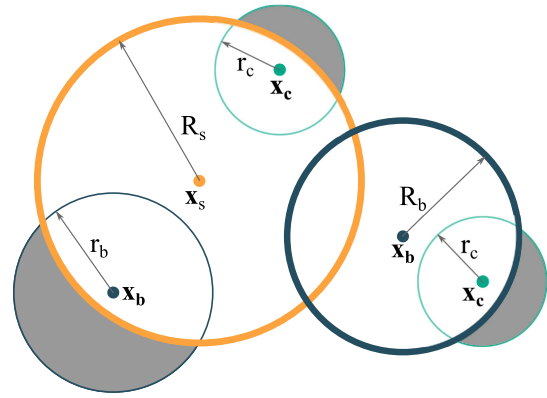


Fig. 11. BPs and cellular BSs within exclusion zones, which can still transmit in the 28-GHz band.

transmitting in sub-6 GHz band is λ_c , while the cellular BS transmitting in 28-GHz band is described by a thinned PPP of density $\tilde{\lambda}_c$. Similarly, the BPs operating in the 6-GHz is described by a PPP of density λ_b ; however, those operating in 28 GHz are described by a thinned PPP of density $\tilde{\lambda}_b$. The thinned PPPs are approximations of poisson hole process (PHP), which is defined formally in the following approximation.

APPROXIMATION 1 If circular holes of radius ρ are cut out of a PPP of density λ , at the points that follow a PPP of density λ_0 , then the remaining points result in a PHP, which can be approximated as a PPP of density $\tilde{\lambda}$, defined as follows:

$$\tilde{\lambda} = \lambda \exp(-\pi\lambda_0\rho^2). \quad (16)$$

In Fig. 11, we show that the BPs and cellular BSs within the exclusion zones can still transmit in the 28-GHz band. As an approximation, we define r_c and r_b as the average distances of the nearest neighbor in PPPs of densities λ_c and λ_b , respectively, which means that on average, a cellular BS can connect to a cellular user r_c distance away. Similarly,

a BP connects to a BP, which is, on average, r_b distance away. In the figure, this is depicted through gray areas. In other words, even if the cellular BSs and BPs lie within exclusion zones, they can still transmit in 28 GHz because they might have users in the gray shaded areas, lying outside the exclusion zones.

LEMMA 5 The average nearest neighbor distance of a PPP of density λ is $\frac{1}{2\sqrt{\lambda}}$.

PROOF The proof follows directly from using the contact distribution $f_{nn}(r) \triangleq 2\pi\lambda r \exp(-\pi\lambda r^2)$. \square

The PHP describing the BPs transmitting in 28-GHz band can be seen as what remains after removing the BPs, which fall inside circles of radius $R_s - r_b$ centered around each ES, i.e., each point in Φ_s . Through Approximation 1, we can define the PHP as a PPP of density $\tilde{\lambda}_b$ as follows:

$$\tilde{\lambda}_b \triangleq \lambda_b \exp(-\pi\lambda_s (R_s - r_b)^2 \mathbb{I}\{R_s > r_b\}), \quad r_b \triangleq \frac{1}{2\sqrt{\lambda_b}}. \quad (17)$$

Similarly, the PHP describing the cellular BSs transmitting in 28-GHz frequencies can be visualized as the points remaining after removing points from circles of radius $R_s - r_c$ centered at each ES in Φ_s and circles of radius $R_b - r_c$ centered around each BP in Φ_b . We approximate this PHP as a PPP of density $\tilde{\lambda}_c$, defined as follows:

$$\tilde{\lambda}_c \triangleq \lambda_c \exp\left(-\pi\lambda_c (R_s - r_c)^2 \mathbb{I}\{R_s > r_c\} - \pi\lambda_b (R_b - r_c)^2 \mathbb{I}\{R_b > r_c\}\right) \quad (18)$$

where $r_c \triangleq \frac{1}{2\sqrt{\lambda_c}}$.

A. Coverage Probability

In the following Lemmas, we present the coverage probability of the cellular BSs and the BPs transmitting in different frequency bands. The proof of these Lemmas is similar to those of Theorems 1 and 2, and is, therefore, skipped.

LEMMA 6 The coverage probability of cellular users in the 28-GHz band is

$$P_c(\tau) = 2\pi\tilde{\lambda}_c \sum_{k=1}^m \binom{m}{k} (-1)^{k+1} \int_0^\infty \exp(-\pi\tilde{\lambda}_c v^2) \times \mathcal{L}_{I_s}(\Omega_c, R_s, \lambda_s) \mathcal{L}_{I_c}(\Omega_c, v, \tilde{\lambda}_c) \mathcal{L}_{I_b}(\Omega_c, R_b, \tilde{\lambda}_b) v dv. \quad (19)$$

LEMMA 7 The coverage probability of cellular users in the sub 6-GHz band is

$$P_{cn}(\tau) = 2\pi\lambda_c \sum_{k=1}^m \binom{m}{k} (-1)^{k+1} \times \int_0^\infty e^{-\pi\lambda_c v^2} \mathcal{L}_{I_c}(\Omega_c, v, \lambda_c) v dv. \quad (20)$$

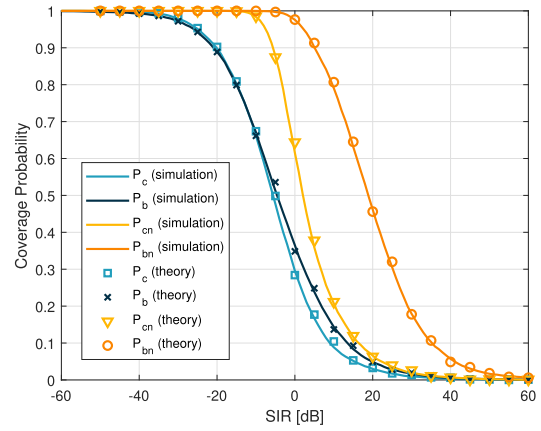


Fig. 12. Coverage probability, simulation versus theory.

LEMMA 8 The coverage probability of BPs in the 28-GHz band is

$$P_b(\tau) = 2\pi\tilde{\lambda}_b \sum_{k=1}^m \binom{m}{k} (-1)^{k+1} \int_0^\infty \exp(-\pi\tilde{\lambda}_b v^2) \times \mathcal{L}_{I_s}(\Omega_b, R_s, \lambda_s) \mathcal{L}_{I_c}(\Omega_b, 0, \tilde{\lambda}_c) \mathcal{L}_{I_b}(\Omega_b, v, \tilde{\lambda}_b) v dv. \quad (21)$$

LEMMA 9 The coverage probability of BPs in the 6-GHz band is

$$P_{bn}(\tau) = 2\pi\lambda_b \sum_{k=1}^m \binom{m}{k} (-1)^{k+1} \times \int_0^\infty e^{-\pi\lambda_b v^2} \mathcal{L}_{I_b}(\Omega_b, v, \lambda_b) v dv. \quad (22)$$

The coverage probability obtained from simulation are in agreement with Lemmas 6–8, as evident from Fig. 12.

B. Average Data Rate

Since the users viz., cellular and BPs, are scattered uniformly in the \mathbb{R}^2 -plane, we need to characterize their data rate as the average of the data rates experienced by the users operating in different frequency bands. We denote the amount of bandwidth offered in 28-GHz, 6-GHz, and sub 6-GHz bands with B , B_{bn} , and B_{cn} , respectively.

THEOREM 3 The average data rate of cellular users is given as follows:

$$D_c(R_s, R_b, \tau) = \left(\exp(-\pi\lambda_s R_s^2 - \pi\tilde{\lambda}_b R_b^2) (BP_c(\tau) - B_{cn}P_{cn}(\tau)) + B_{cn}P_{cn}(\tau) \right) \log_2(1 + \tau). \quad (23)$$

PROOF The average data rate of the cellular users operating in 28-GHz band is $P_c(\tau)B \log_2(1 + \tau)$ and of those operating in sub 6-GHz is $P_{cn}(\tau)B_{cn} \log_2(1 + \tau)$. Moreover, the fraction of cellular users operating in 28-GHz band is $e^{-\pi\lambda_s R_s^2 - \pi\tilde{\lambda}_b R_b^2}$. On taking the average over the fraction of cellular users operating in the 28-GHz and sub 6-GHz

frequency, we get the expression in (23), which concludes the proof.

THEOREM 4 The average data rate of BPs is given as follows:

$$D_b(R_s, R_b, \tau) = \left(e^{-\pi\lambda_s R_s^2} (B P_b(\tau) - B_{bn} P_{bn}(\tau)) + B_{bn} P_{bn}(\tau) \right) \log_2(1 + \tau). \quad (24)$$

PROOF The proof is similar to that of Theorem 3 and is, therefore, skipped. \square

VI. DATA RATE OPTIMIZATION AND RESULTS

In this section, we define the problem of joint data rate maximization of the two terrestrial networks. We then approximate the data rate expressions as closed-form sigmoid curves and then present the optimization results, i.e., report the optimal radii of the exclusion zones.

A. Problem Formulation

The goal of this article is to improve the performance of the terrestrial users in terms of their data rate by managing the interference through the adoption of exclusion zones of certain radii. In other words, we aim to find the radii of the exclusion zones, which improve the data rate of the cellular users and BPs. For this, we define two objective functions. The first one is the sum of data rates $f_\Sigma \triangleq D_c + D_b$, and the other is the product of data rates $f_\Pi \triangleq D_c \cdot D_b$.

Problem 1:

$$\underset{(R_s, R_b) \in \mathbb{R}^+ \times \mathbb{R}^+}{\text{maximize}} \quad f_\Sigma(R_s, R_b, \tau) = D_c + D_b. \quad (25)$$

Problem 2:

$$\underset{(R_s, R_b) \in \mathbb{R}^+ \times \mathbb{R}^+}{\text{maximize}} \quad f_\Pi(R_s, R_b, \tau) = D_c D_b. \quad (26)$$

In Problem 1, we try to maximize the sum of the data rates in which the data rate of one network can be sacrificed to improve the data rate of another network. However, in Problem 2, this is prevented as the product of two opposing terms, which is maximum only when the two terms are equal. So, the data rate of one network will not be sacrificed to increase the data rate of another, thereby ensuring fairness in data rate.

These problems appear simple. However, the only way to solve them directly is through exhaustive search, as the coverage probability expressions P_c, P_b, P_{cn} , and P_{bn} , are not available in closed form. To expedite the optimization process, we approximate the coverage probability expressions as sigmoid curves that are function of R_s and R_b for a given τ . The approximation technique is described in detail in the following subsection VI-B.

B. Sigmoid Approximation

Consider that we have a coverage probability expression $p(\tau|\mathbf{x}) \triangleq \mathbb{P}(\text{SIR} > \tau | \mathbf{x})$, where τ is the SIR threshold, and \mathbf{x} is a vector of parameters. Often times, deriving

coverage expressions using stochastic geometry results in complicated expressions involving several integrals, which make it computation intensive and difficult to analyze the trends with respect to the variables of the system model.

This motivates us to come up with a closed-form expression for $p(\tau, \mathbf{x})$, which depends on several variables denoted by the vector $\mathbf{x} \in \mathcal{V} \subseteq \mathbb{R}^d$. The goal is to be able to use the coverage expression in objective functions that can be optimized through gradient descent methods, in contrast to exhaustive search, thereby cutting down on computation time.

We start with the assumption that the SIR has a logistic distribution [53], which allows us to express the cumulative distribution function (CDF) of SIR, i.e., $\mathbb{P}(\text{SIR} \leq \tau)$ as a sigmoid function. We are interested in determining the coverage probability, which is the complementary CDF of the SIR, which is also a sigmoid function.³ The sigmoid curve is a natural choice to approximate the coverage probability expression as the domain $\in \mathbb{R}$ and range $\in [0, 1]$. The function is closed form and differentiable, which makes calculations easier. For example, Al-Hourani et al. [54] use sigmoid curve to approximate the line-of-sight probability CDF as a function of the elevation angle. The CDF2PDF method in [55] employs a shallow neural network with one hidden layer having sigmoid activation functions and one linear output node, for CDF estimation.

We approximate $p(\tau, \mathbf{x})$ as a sigmoid function of τ as follows:

$$p_1(\tau|\mathbf{x}) = \sigma(-w_1(\mathbf{x})\tau - w_0(\mathbf{x})) \quad (27)$$

where τ is in dB scale, $\sigma(\cdot)$ is the sigmoid function, $w_1(\mathbf{x}) \in \mathbb{R}$ is the weight, and $w_0(\mathbf{x}) \in \mathbb{R}$ is the bias. We call $p_1(\tau|\mathbf{x}) \approx p(\tau|\mathbf{x})$ *sigmoid-I approximation*.

Using the data points $\{\log(p(\tau|\mathbf{x})^{-1} - 1), \tau\}$ for a given \mathbf{x} , we perform linear regression [56] and obtain $p_1(\tau|\mathbf{x})$ ⁴ thereby generating the set of data points $\{\mathbf{x}, w_1(\mathbf{x}), w_0(\mathbf{x})\}$.

REMARK 1 The time complexity of sigmoid-I approximation is $\mathcal{O}(|\mathcal{D}_\tau|)$, where $\tau \in \mathcal{D}_\tau$.

The next step involves approximating the weight $w_1(\mathbf{x})$ and bias $w_0(\mathbf{x})$ through nonlinear regression with n basis functions.

DEFINITION 4 The nonlinear regression function $f_w : \mathbb{R}^d \times \mathbb{R}^{(n+1) \times d} \rightarrow \mathbb{R}$ is defined as follows:

$$f_w(\mathbf{x}, \mathbf{A}) = \mathbf{1}_{n+1}^\top (\mathbf{A} \odot \mathbf{M}(\{\phi_i\}_{i=1}^n, \mathbf{x})) \mathbf{1}_d \quad (28)$$

where $\phi_j(\cdot)$ is the j th basis function; $\mathbf{X} \odot \mathbf{Y}$ denotes the Hadamard product of \mathbf{X} and \mathbf{Y} ; $\mathbf{A} \in \mathbb{R}^{(n+1) \times d}$, and

$$\mathbf{M}(\{\phi_i\}_{i=1}^n, \mathbf{x}) \triangleq \begin{bmatrix} 1 & \dots & 1 & \dots & 1 \\ \phi_1(\mathbf{x}_1) & \dots & \phi_1(\mathbf{x}_j) & \dots & \phi_1(\mathbf{x}_d) \\ \vdots & & \vdots & & \vdots \\ \phi_n(\mathbf{x}_1) & \dots & \phi_n(\mathbf{x}_j) & \dots & \phi_n(\mathbf{x}_d) \end{bmatrix}.$$

³ $1 - \sigma(ax + b) = \sigma(-ax - b)$.

⁴ where $\epsilon < p(\tau|\mathbf{x}) < 1 - \epsilon$, where $\epsilon > 0$, to avoid extremely large values.

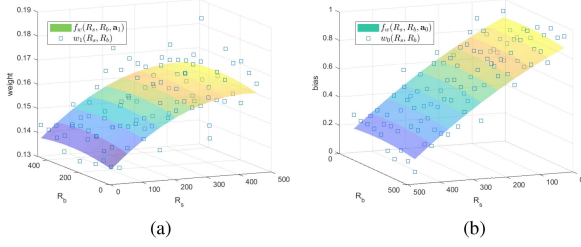


Fig. 13. Regression surface f_w . (a) $w_1(R_s, R_b)$ regression. (b) $w_0(R_s, R_b)$ regression.

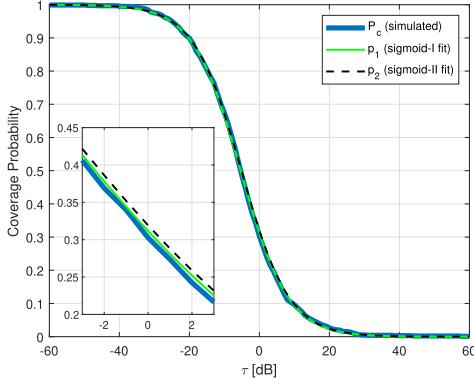


Fig. 14. Comparing sigmoid fit with simulated coverage probability. $R_s = 110$ m and $R_b = 10$ m.

We approximate $w_1(\mathbf{x}) \approx f_w(\mathbf{x}, \mathbf{A}_1)$ and $w_0(\mathbf{x}) \approx f_w(\mathbf{x}, \mathbf{A}_0)$. Therefore, the coverage probability can be expressed as follows:

$$p_2(\tau, \mathbf{x}) = \sigma(-f_w(\mathbf{x}, \mathbf{A}_1)\tau - f_w(\mathbf{x}, \mathbf{A}_0)). \quad (29)$$

We call $p_2(\tau, \mathbf{x}) \approx p_1(\tau|\mathbf{x})$ *sigmoid-II* approximation.

REMARK 2 The time complexity of sigmoid-II approximation is $\mathcal{O}(|\mathcal{D}_x|(n+1)^3 d^3)$, where $\mathbf{x} \in \mathcal{D}_x$.

In Fig. 13, we show the surfaces $f_w(\mathbf{x}, \mathbf{A}_1)$ and $f_w(\mathbf{x}, \mathbf{A}_0)$ that fit the data points of weight w_1 and bias w_0 of sigmoid-I fit, respectively. We define $\mathbf{x} \triangleq [R_s R_b]^\top$, and $\phi_1(t) = t$ and $\phi_2(t) = t^2$. In Fig. 14, we show how the sigmoid fit curves compare with the simulated coverage probability curve. We quantify the root mean square error (RMSE) between the simulated coverage probability curve with the sigmoid fit curves in Fig. 15, establishing the utility of our approach.

C. Optimization Results

We first obtain the closed-form expressions of the coverage probability P_c through sigmoid-II fit denoted by \hat{P}_c . Then, the approximate average data rates \hat{D}_c can be expressed as follows. The average data rate of the cellular users is

$$\hat{D}_c(R_s, R_b, \tau) = \left(e^{-\pi\lambda_s R_s^2 - \pi\tilde{\lambda}_b R_b^2} (B\hat{P}_c(\tau) - B_{cn}\hat{P}_{cn}(\tau)) + B_{cn}\hat{P}_{cn}(\tau) \right) \log_2(1 + \tau). \quad (30)$$

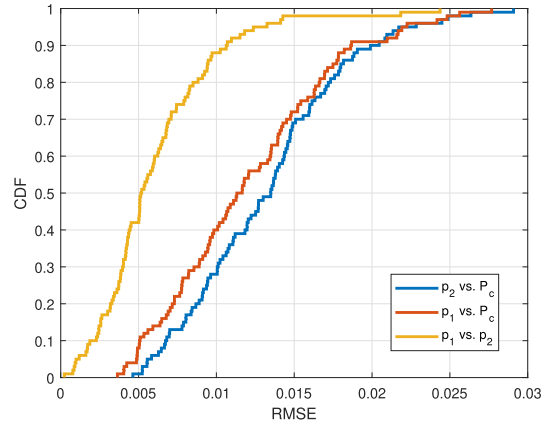


Fig. 15. CDF of the RMSE between the simulated coverage probability curve and the sigmoid fits.

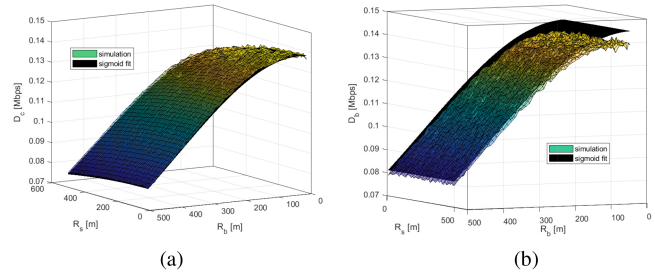


Fig. 16. Comparing simulated data rates with sigmoid fit data rates. (a) $D_c(R_s, R_b)$. (b) $D_b(R_s, R_b)$.

Similarly, the average data rate of the BPs is

$$\hat{D}_b(R_s, R_b, \tau) = \left(e^{-\pi\lambda_s R_s^2} (B\hat{P}_b(\tau) - B_{bn}\hat{P}_{bn}(\tau)) + B_{bn}\hat{P}_{bn}(\tau) \right) \log_2(1 + \tau). \quad (31)$$

In Fig. 16, we compare the data rate curves obtained through simulations with those obtained from the closed-form expressions in (30) and (31), and we observe that the surfaces overlap.

In Fig. 17, we show the position of the maxima for objectives f_Σ and f_Π for different values of bandwidth ratio B/B_{cn} . The bandwidth ratio is the ratio between the bandwidth offered by 28-GHz band and that offered by sub-6 GHz or 6 GHz. We perform the optimization through gradient descent methods. Having exclusion zones helps in decreasing the interference in 28 GHz, but if the radii of the exclusion zones are too big then the signal strength too is decreased, as the density of the transmitters in 28 GHz decreases. Therefore, we could find optimal values of R_s and R_b , which maximize the sum or product of data rates.

In Fig. 18, we show the improvements in the data rate as the bandwidth ratio increases. We measure the improvement with respect to the absence of exclusion zones, i.e., $R_s = 0$ m and $R_b = 0$ m. We see that the improvement saturates at $\sim 5\%$ for cellular users, as we increase the bandwidth ratio, and for BPs, instead of improvement, the data rate worsens by $\sim 1\%$. When we have similar bandwidths, we see up to

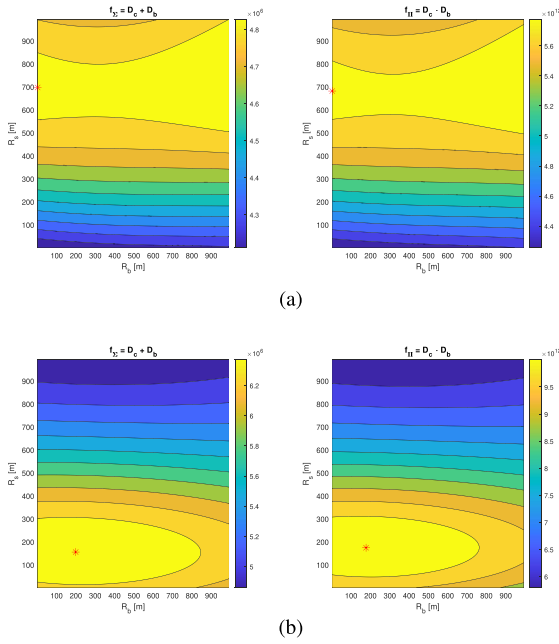


Fig. 17. Optimization results for different values of B/B_{cn} . (a) $B/B_{cn} = 1$. (b) $B/B_{cn} = 1.5$.

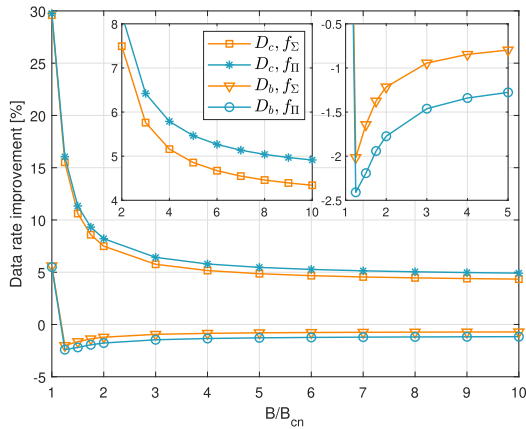


Fig. 18. Data rate improvement versus bandwidth ratio.

30% improvement for cellular users and 5% improvement for BPs.

D. Complexity Analysis

From the location databases, we get the set of ES locations as \mathcal{V}_{ES} , cellular BS locations as \mathcal{V}_{BS} , and BP locations as \mathcal{V}_{BP} . Now, we list down each step in the process, as depicted in Fig. 2, and calculate its corresponding computational complexity.

- S_1 . *PPP approximation*: This step involves counting the number of points in each set $\mathcal{V}_{(\cdot)}$ and the area of the convex hull of those points. The time complexity is $\mathcal{O}(q \log_2 q)$, where $q = \max\{|\mathcal{V}_{ES}|, |\mathcal{V}_{BS}|, |\mathcal{V}_{BP}|\}$.
- S_2 . *Data rate evaluation*: Let $R_s \in \mathcal{D}_{R_s}$ and $R_b \in \mathcal{D}_{R_b}$, and $\tau \in \mathcal{D}_{\tau}$, then we perform $|\mathcal{D}_{R_s} \times \mathcal{D}_{R_b} \times \mathcal{D}_{\tau}|$

function evaluations, each of which take constant time. So, the complexity of this step is $\mathcal{O}(|\mathcal{D}_{R_s}| |\mathcal{D}_{R_b}| |\mathcal{D}_{\tau}|)$.

- S_3 . *Sigmoid-I approximation*: $\mathcal{O}(|\mathcal{D}_{\tau}|)$ from Remark 1.
- S_4 . *Sigmoid-II approximation*: $\mathcal{O}(|\mathcal{D}_{R_s}| |\mathcal{D}_{R_b}|)$ from Remark 2.
- S_5 . *Joint data rate maximization*: Since the number of variables is fixed, the time complexity is $\mathcal{O}(1)$.
- S_6 . *Frequency allocation*: The BPs first check against each ESs and choose to operate in 28 GHz if they are not within the exclusion zone of any ES. Then, the BPs follow suit and check against all the ESs and BPs. The complexity is $\mathcal{O}(|\mathcal{V}_{BP}| |\mathcal{V}_{ES}| + |\mathcal{V}_{BP}| |\mathcal{V}_{BS}| + |\mathcal{V}_{ES}| |\mathcal{V}_{BS}|)$.

We can see that S_2 dominates S_3 and S_4 . Moreover, S_6 dominates S_1 . Therefore, the overall complexity of the process is simply the complexity of $S_2 \cup S_6$, i.e., $\mathcal{O}(\max\{|\mathcal{V}_{BP}| |\mathcal{V}_{ES}| + |\mathcal{V}_{BP}| |\mathcal{V}_{BS}| + |\mathcal{V}_{ES}| |\mathcal{V}_{BS}|, |\mathcal{D}_{R_s}| |\mathcal{D}_{R_b}| |\mathcal{D}_{\tau}|\})$.

When the exclusion zone radii are fixed to suboptimal values, without ensuring that the data rate can be jointly maximized for a given environment, the complexity of the frequency allocation task is still the same as S_6 . When the frequency allocation is done in a combinatorial way to maximize the data rate, the complexity is $\mathcal{O}(2^{|\mathcal{V}_{BP}| + |\mathcal{V}_{BS}|})$.

VII. CONCLUSION

In this article, we minimized the interference caused by the Earth-to-satellite transmissions on the terrestrial users through exclusion zones. In practice, this can be deployed using a spectrum access database, where the location of the ESs and BPs is updated regularly, and based on the current location of the terrestrial users, they are allowed to receive signals in a particular frequency, as per the rules. We quantified the performance of terrestrial users in terms of average data rate by employing tools from stochastic geometry. The theoretical expressions were verified through Monte-Carlo simulations and converted into closed-form expressions through two-step sigmoid approximation. The approximation method presented in this work can be useful for the research community, as any complicated coverage probability curve can be approximated as a sigmoid curve by the use of appropriate basis functions.

The work can be further generalized by considering users that are capable of operating in several frequency bands, and based on the current interference from the surroundings, can choose a frequency band that offers the highest QoS. This would require modeling each user as an agent in a multiagent game setting.

APPENDIX

A. Proof of Lemma 2

The interference from the ESs can be expressed as follows:

$$I_s \triangleq \sum_{\mathbf{x} \in \Phi_s} HG(\alpha) p_s \|\mathbf{x}\|^{-\zeta} \quad (32)$$

where $H \sim \Gamma(m, \frac{1}{m})$ because of Nakagami- m fading channel, $\alpha \sim f_{\alpha_0}$, and Φ_s is a PPP of intensity λ_s .

PROOF The Laplace transform of I_s is

$$\mathcal{L}_{I_s}(s) = \mathbb{E}_{H, \Phi_s, \alpha} [\exp(-sI_s)] \quad (33)$$

$$= \mathbb{E}_{H, \Phi_s, \alpha} \left[\exp \left(-s \sum_{\mathbf{x} \in \Phi_s} HG(\alpha) p_s \|\mathbf{x}\|^{-\zeta} \right) \right] \quad (34)$$

$$= \mathbb{E}_{H, \Phi_s, \alpha} \left[\prod_{\mathbf{x} \in \Phi_s} \exp(-sHG(\alpha)p_s \|\mathbf{x}\|^{-\zeta}) \right] \quad (35)$$

$$\stackrel{(a)}{=} \mathbb{E}_{\alpha} \left[\exp \left(-2\pi\lambda_s \int_v^\infty (1 - \mathbb{E}_H [\exp(-sHG(\alpha)p_s x^{-\zeta})]) x dx \right) \right] \quad (36)$$

$$\stackrel{(b)}{=} \int_0^\pi \exp \left(-2\pi\lambda_s \int_v^\infty \left\{ 1 - \left(1 + \frac{G(\alpha)p_s x^{-\zeta}}{m} s \right)^{-m} \right\} x dx \right) f_{\alpha_0}(\alpha) d\alpha \quad (37)$$

where step (a) follows from definition of a probability generating functional (PGFL) [27] and step (b) follows from the moment generating function (MGF) of a Gamma distributed random variable [57]. \square

B. Proof of Lemma 3

The interference from the BPs can be expressed as follows:

$$I_b \triangleq \sum_{\mathbf{x} \in \Phi_b} HG p_b \|\mathbf{x}\|^{-\zeta} \quad (38)$$

where $H \sim \Gamma(m, \frac{1}{m})$ because of Nakagami- m fading channel, Φ_s is a PPP of intensity λ_b , and G is a discrete random variable with $f_G(G_1) = \frac{\Theta}{\pi}$ and $f_G(G_0) = 1 - \frac{\Theta}{\pi}$.

PROOF The Laplace transform of I_b is

$$\mathcal{L}_{I_b}(s) = \mathbb{E}_{H, \Phi_b, G} [\exp(-sI_b)] \quad (39)$$

$$= \mathbb{E}_{H, \Phi_b, G} \left[\exp \left(-s \sum_{\mathbf{x} \in \Phi_b} HG p_b \|\mathbf{x}\|^{-\zeta} \right) \right] \quad (40)$$

$$= \mathbb{E}_{H, \Phi_b, G} \left[\prod_{\mathbf{x} \in \Phi_b} \exp(-sHG p_b \|\mathbf{x}\|^{-\zeta}) \right] \quad (41)$$

$$\stackrel{(a)}{=} \exp \left(\mathbb{E}_G \left[-2\pi\lambda_b \int_v^\infty (1 - \mathbb{E}_H [\exp(-sHG p_b x^{-\zeta})]) x dx \right] \right) \quad (42)$$

$$\stackrel{(b)}{=} \exp \left(\mathbb{E}_G \left[-2\pi\lambda_s \int_v^\infty \left\{ 1 - \left(1 + \frac{G p_b x^{-\zeta}}{m} s \right)^{-m} \right\} x dx \right] \right) \quad (43)$$

$$= \exp \left(-2\pi\lambda_s \frac{\Theta}{\pi} \int_v^\infty \left\{ 1 - \left(1 + \frac{G_1 p_b x^{-\zeta}}{m} s \right)^{-m} \right\} x dx \right)$$

$$\times \exp \left(-2\pi\lambda_s \left(1 - \frac{\Theta}{\pi} \right) \int_v^\infty \left\{ 1 - \left(1 + \frac{G_0 p_b x^{-\zeta}}{m} s \right)^{-m} \right\} x dx \right) \quad (44)$$

where step (a) follows from the definition of a PGFL, and step (b) follows from the MGF of a Gamma distributed random variable. \square

REMARK 3 The proof of Lemma 4 is skipped because it is similar to the proof of Lemma 3 with $G = 1$.

ACKNOWLEDGMENT

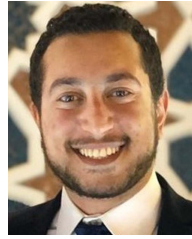
The work was conducted when Aniq Ur Rahman was enrolled as a Master of Science (M.S.) student with KAUST, Saudi Arabia.

REFERENCES

- [1] S. Dang, O. Amin, B. Shihada, and M.-S. Alouini, "What should 6G be?," *Nature Electron.*, vol. 3, no. 1, pp. 20–29, 2020.
- [2] O. Kodheli et al., "Satellite communications in the new space era: A survey and future challenges," *IEEE Commun. Surv. Tut.*, vol. 23, no. 1, pp. 70–109, Jan./Mar. 2021.
- [3] O. Kodheli, A. Guidotti, and A. Vanelli-Coralli, "Integration of satellites in 5G through LEO constellations," in *Proc. GLOBECOM IEEE Glob. Commun. Conf.*, 2017, pp. 1–6.
- [4] A. U. Rahman, F. Fourati, K.-H. Ngo, A. Jindal, and M.-S. Alouini, "Network graph generation through adaptive clustering and infection dynamics: A step toward global connectivity," *IEEE Commun. Lett.*, vol. 26, no. 4, pp. 783–787, Apr. 2022.
- [5] P. Wang, B. Di, and H. Zhang, "Mega-constellation design for integrated satellite-terrestrial networks for global seamless connectivity," *IEEE Wireless Commun. Lett.*, vol. 11, no. 8, pp. 1669–1673, Aug. 2022.
- [6] B. Al Homssi et al., "Next generation mega satellite networks for access equality: Opportunities, challenges, and performance," *IEEE Commun. Mag.*, vol. 60, no. 4, pp. 18–24, Apr. 2022.
- [7] B. Di, L. Song, Y. Li, and H. V. Poor, "Ultra-dense LEO: Integration of satellite access networks into 5G and beyond," *IEEE Wireless Commun.*, vol. 26, no. 2, pp. 62–69, Apr. 2019.
- [8] T. Wang, Z. Qian, L. Kang, S. Geng, and X. Zhao, "Coexistence interference analysis of 28GHz IMT and fixed-satellite service systems," in *Proc. IEEE 2nd Adv. Inf. Technol., Electron. Autom. Control Conf.*, 2017, pp. 1574–1578.
- [9] T. Miller, Y. S. Chan, V. Jervis, S. Kirtay, and A. Kaur, "Expanding digital connectivity through satellite broadband in the 28GHz band," Plum Consulting, Tech. Rep., Oct. 2021. [Online]. Available: <https://plumconsulting.co.uk/expanding-digital-connectivity-through-satellite-broadband-in-the-28-GHz-band/>
- [10] S. P. Winter and A. Knopp, "Modeling of fixed service interference in aeronautical SATCOM channels," *IEEE Trans. Aerosp. Electron. Syst.*, vol. 58, no. 2, pp. 942–961, Apr. 2022.
- [11] 3GPP, "Solutions for NR to support non-terrestrial networks (NTN)," 3GPP, Tech. Rep. TR 38.821, Dec. 2019. [Online]. Available: <https://portal.3gpp.org/desktopmodules/Specifications/SpecificationDetails.aspx?specificationId=3525>
- [12] GSMA and ABI Research, "Mobile backhaul options: Spectrum analysis and recommendations," *GSMA, Tech. Rep.*, Sep. 2018. [Online]. Available: <https://www.gsma.com/spectrum/wp-content/uploads/2019/04/Mobile-Backhaul-Options.pdf>

- [13] B. Wang and K. R. Liu, "Advances in cognitive radio networks: A survey," *IEEE J. Sel. Topics Signal Process.*, vol. 5, no. 1, pp. 5–23, Feb. 2011.
- [14] S. Haykin, D. J. Thomson, and J. H. Reed, "Spectrum sensing for cognitive radio," *Proc. IEEE*, vol. 97, no. 5, pp. 849–877, May 2009.
- [15] Y.-E. Lin, K.-H. Liu, and H.-Y. Hsieh, "On using interference-aware spectrum sensing for dynamic spectrum access in cognitive radio networks," *IEEE Trans. Mobile Comput.*, vol. 12, no. 3, pp. 461–474, Mar. 2013.
- [16] P. J. Kolodzy, "Interference temperature: A metric for dynamic spectrum utilization," *Int. J. Netw. Manage.*, vol. 16, no. 2, pp. 103–113, 2006.
- [17] A. Kaur and K. Kumar, "A comprehensive survey on machine learning approaches for dynamic spectrum access in cognitive radio networks," *J. Exp. Theor. Artif. Intell.*, vol. 34, no. 1, pp. 1–40, 2022.
- [18] F. Paisana et al., "Context-aware cognitive radio using deep learning," in *Proc. IEEE Int. Symp. Dyn. Spectr. Access Netw.*, 2017, pp. 1–2.
- [19] Y. Wang, M. Liu, J. Yang, and G. Gui, "Data-driven deep learning for automatic modulation recognition in cognitive radios," *IEEE Trans. Veh. Technol.*, vol. 68, no. 4, pp. 4074–4077, Apr. 2019.
- [20] H. Xing, H. Qin, S. Luo, P. Dai, L. Xu, and X. Cheng, "Spectrum sensing in cognitive radio: A deep learning based model," *Trans. Emerg. Telecommun. Technol.*, vol. 33, no. 1, 2022, Art. no. e4388.
- [21] H. Albinsaid, K. Singh, S. Biswas, and C.-P. Li, "Multi-agent reinforcement learning based distributed dynamic spectrum access," *IEEE Trans. Cogn. Commun. Netw.*, vol. 8, no. 2, pp. 1174–1185, Jun. 2022.
- [22] X. Tan et al., "Cooperative multi-agent reinforcement learning based distributed dynamic spectrum access in cognitive radio networks," *IEEE Internet Things J.*, vol. 9, no. 19, pp. 19477–19488, Oct. 2022.
- [23] A. Kaur and K. Kumar, "Imperfect CSI based intelligent dynamic spectrum management using cooperative reinforcement learning framework in cognitive radio networks," *IEEE Trans. Mobile Comput.*, vol. 21, no. 5, pp. 1672–1683, May 2022.
- [24] A. Ur Rahman, M. A. Kishk, and M.-S. Alouini, "A game-theoretic framework for coexistence of WiFi and cellular networks in the 6-GHz unlicensed spectrum," *IEEE Trans. Cognit. Commun. Netw.*, vol. 9, no. 1, pp. 239–251, Feb. 2023.
- [25] J. Wang, G. Scutari, and D. P. Palomar, "Robust MIMO cognitive radio via game theory," *IEEE Trans. Signal Process.*, vol. 59, no. 3, pp. 1183–1201, Mar. 2011.
- [26] D. Niyato and E. Hossain, "A game-theoretic approach to competitive spectrum sharing in cognitive radio networks," in *Proc. IEEE Wireless Commun. Netw. Conf.*, 2007, pp. 16–20.
- [27] M. Haenggi, J. G. Andrews, F. Baccelli, O. Dousse, and M. Franceschetti, "Stochastic geometry and random graphs for the analysis and design of wireless networks," *IEEE J. Sel. Areas Commun.*, vol. 27, no. 7, pp. 1029–1046, Sep. 2009.
- [28] H. ElSawy, A. Sultan-Salem, M.-S. Alouini, and M. Z. Win, "Modeling and analysis of cellular networks using stochastic geometry: A tutorial," *IEEE Commun. Surv. Tut.*, vol. 19, no. 1, pp. 167–203, Jan./Mar. 2017.
- [29] J. G. Andrews, A. K. Gupta, and H. S. Dhillon, "A primer on cellular network analysis using stochastic geometry," 2016, *arXiv:1604.03183*.
- [30] P. C. Pinto, A. Giorgetti, M. Z. Win, and M. Chiani, "A stochastic geometry approach to coexistence in heterogeneous wireless networks," *IEEE J. Sel. Areas Commun.*, vol. 27, no. 7, pp. 1268–1282, Sep. 2009.
- [31] A. Mbengue and Y. Chang, "Performance analysis of LAA/Wi-Fi coexistence: Stochastic geometry model," in *Proc. IEEE Wireless Commun. Netw. Conf.*, 2018, pp. 1–6.
- [32] A. Bhorkar, C. Ibars, and P. Zong, "Performance analysis of LTE and Wi-Fi in unlicensed band using stochastic geometry," in *Proc. IEEE 25th Annu. Int. Symp. Personal, Indoor, Mobile Radio Commun.*, 2014, pp. 1310–1314.
- [33] A. U. Rahman, M. A. Kishk, and M.-S. Alouini, "Improving spectral efficiency of wireless networks through democratic spectrum sharing," 2021, *arXiv:2111.10570*.
- [34] M. A. Kishk and H. S. Dhillon, "Coexistence of RF-powered IoT and a primary wireless network with secrecy guard zones," *IEEE Trans. Wireless Commun.*, vol. 17, no. 3, pp. 1460–1473, Mar. 2018.
- [35] S. K. Sharma, S. Chatzinotas, and B. Ottersten, "Transmit beamforming for spectral coexistence of satellite and terrestrial networks," in *Proc. 8th Int. Conf. Cogn. Radio Oriented Wireless Netw.*, 2013, pp. 275–281.
- [36] E. Lagunas, C. G. Tsinos, S. K. Sharma, and S. Chatzinotas, "5G cellular and fixed satellite service spectrum coexistence in C-band," *IEEE Access*, vol. 8, pp. 72078–72094, 2020.
- [37] Y. Cho, H.-K. Kim, M. Nekovee, and H.-S. Jo, "Coexistence of 5G with satellite services in the millimeter-wave band," *IEEE Access*, vol. 8, pp. 163618–163636, 2020.
- [38] W. A. Hassan, H.-S. Jo, and A. R. Tharek, "The feasibility of coexistence between 5G and existing services in the IMT-2020 candidate bands in Malaysia," *IEEE Access*, vol. 5, pp. 14867–14888, 2017.
- [39] Y. Cho, H. Kim, E. E. Ahiagbe, and H.-S. Jo, "Spectral coexistence of IMT-2020 with fixed-satellite service in the 27-27.5GHz band," in *Proc. Int. Conf. Inf. Commun. Technol. Convergence*, 2018, pp. 1–6.
- [40] S. Kim, E. Visotsky, P. Moorut, K. Bechta, A. Ghosh, and C. Dietrich, "Coexistence of 5G with the incumbents in the 28 and 70GHz bands," *IEEE J. Sel. areas Commun.*, vol. 35, no. 6, pp. 1254–1268, Jun. 2017.
- [41] H. Zafar, B. Evans, and A. Mohamed, "Coexistence between 5G new radio downlink and fixed satellite service uplink in millimetre-wave band," in *Proc. Ka Broadband Commun. Conf.*, 2021. [Online]. Available: <https://proceedings.kaconf.com/>
- [42] Z. Lin, M. Lin, B. Champagne, W.-P. Zhu, and N. Al-Dhahir, "Secrecy-energy efficient hybrid beamforming for satellite-terrestrial integrated networks," *IEEE Trans. Commun.*, vol. 69, no. 9, pp. 6345–6360, Sep. 2021.
- [43] Y. Yan, K. An, B. Zhang, W.-P. Zhu, G. Ding, and D. Guo, "Outage-constrained robust multigroup multicast beamforming for satellite-based Internet of Things coexisting with terrestrial networks," *IEEE Internet Things J.*, vol. 8, no. 10, pp. 8159–8172, May 2021.
- [44] A. Talgat, M. A. Kishk, and M.-S. Alouini, "Stochastic geometry-based analysis of LEO satellite communication systems," *IEEE Commun. Lett.*, vol. 25, no. 8, pp. 2458–2462, Aug. 2021.
- [45] N. Okati, T. Riihonen, D. Korpi, I. Angervo, and R. Wichman, "Downlink coverage and rate analysis of low Earth orbit satellite constellations using stochastic geometry," *IEEE Trans. Commun.*, vol. 68, no. 8, pp. 5120–5134, Aug. 2020.
- [46] T. A. Khan and M. Afshang, "A stochastic geometry approach to doppler characterization in a LEO satellite network," in *Proc. IEEE Int. Conf. Commun.*, 2020, pp. 1–6.
- [47] R. Wang, M. A. Kishk, and M.-S. Alouini, "Evaluating the accuracy of stochastic geometry based models for LEO satellite networks analysis," *IEEE Commun. Lett.*, vol. 26, no. 10, pp. 2440–2444, Oct. 2022.
- [48] ITU-R, "Reference radiation pattern for earth station antennas in the fixed-satellite service for use in coordination and interference assessment in the frequency range from 2 to 31GHz," vol. 2, 2010, Art. no. 465.
- [49] A. Al-Hourani, "An analytic approach for modeling the coverage performance of dense satellite networks," *IEEE Wireless Commun. Lett.*, vol. 10, no. 4, pp. 897–901, Apr. 2021.
- [50] C. Braun, A. M. Voicu, L. Simić, and P. Mähönen, "Should we worry about interference in emerging dense NGSO satellite constellations?," in *Proc. IEEE Int. Symp. Dyn. Spectr. Access Netw.*, 2019, pp. 1–10.
- [51] FCC, "Schedule S," Accessed on: May 23, 2023. [Online]. Available: <http://https://licensing.fcc.gov/cgi-bin/ws.exe/prod/ib/forms/reports/swr030b.hts?set=>
- [52] M. Alzenad and H. Yanikomeroglu, "Coverage and rate analysis for vertical heterogeneous networks (VHetNets)," *IEEE Trans. Wireless Commun.*, vol. 18, no. 12, pp. 5643–5657, Dec. 2019.
- [53] N. L. Johnson, S. Kotz, and N. Balakrishnan, *Continuous Univariate Distributions*, vol. 2. Hoboken, NJ, USA: Wiley, 1995.

- [54] A. Al-Hourani, S. Kandeepan, and S. Lardner, "Optimal LAP altitude for maximum coverage," *IEEE Wireless Commun. Lett.*, vol. 3, no. 6, pp. 569–572, Dec. 2014.
- [55] S. Zhang, "From CDF to PDF—A density estimation method for high dimensional data," 2018, *arXiv:1804.05316*.
- [56] C. M. Bishop and N. M. Nasrabadi, *Pattern Recognition and Machine Learning*, vol. 4. Berlin, Germany: Springer, 2006.
- [57] D. P. Bertsekas and J. N. Tsitsiklis, *Introduction to Probability*, vol. 1. Nashua, NH, USA: Athena Scientific, 2008.



Mustafa A. Kishk (Member, IEEE) received the B.Sc. and M.Sc. degrees from Cairo University, Giza, Egypt, in 2013 and 2015, respectively, and the Ph.D. degree from Virginia Tech, Blacksburg, VA, USA, in 2018, all in electrical engineering.

From 2019 to 2022, he was a Postdoctoral Research Fellow with the King Abdullah University of Science and Technology, Thuwal, Saudi Arabia. He is an Assistant Professor with Maynooth University, Maynooth, Ireland. His

research interests include UAV communications, satellite communications, and global connectivity for rural and remote areas.



Aniq Ur Rahman received the B.Tech degree in electronics and communication engineering from the National Institute of Technology Durgapur, Durgapur, India, in 2019, and the M.Sc. degree in electrical and computer engineering from the King Abdullah University of Science and Technology, Thuwal, Saudi Arabia, in 2022. He is currently working toward the Dr. Phil. degree in engineering science with Information and Network Science Lab, University of Oxford, Oxford, U.K.

He was selected among 200 young researchers worldwide to attend the 7th Heidelberg Laureate Forum in Heidelberg, Germany.



Mohamed-Slim Alouini (Fellow, IEEE) was born in Tunis, Tunisia. He received the Ph.D. degree in electrical engineering from the California Institute of Technology (CalTech), Pasadena, CA, USA, in 1998.

He served as a faculty member of the University of Minnesota, USA, then with the Texas A&M University at Qatar, Qatar, before joining the King Abdullah University of Science and Technology, Saudi Arabia, as a Professor of electrical engineering in 2009. His current

research interests include the modeling, design, and performance analysis of wireless communication systems.